Journal of Alloys and Compounds 509 (2011) 7639–7644

Contents lists available at ScienceDirect

Journal of Alloys and Compounds

journal homepage: www.elsevier.com/locate/jallcom

Synthesis, morphology, microstructure and magnetic properties of hematite submicron particles

Marin Tadić[a,*], Nada Čitaković[b], Matjaž Panjan[c], Zoran Stojanović[d], Dragana Marković[a], Vojislav Spasojević[a]

[a] Condensed Matter Physics Laboratory, Vinca Institute, University of Belgrade, POB 522, 11001 Belgrade, Serbia
[b] Military Academy, Generala Pavla Jurišića Šturma 33, 11000 Belgrade, Serbia
[c] Jožef Stefan Institute, Jamova 39, 1000 Ljubljana, Slovenia
[d] Institute of Technical Sciences, Serbian Academy of Arts and Sciences, Knez Mihajlova 35/IV, 11000 Belgrade, Serbia

ARTICLE INFO

Article history:
Received 10 February 2011
Received in revised form 21 April 2011
Accepted 21 April 2011
Available online 30 April 2011

Keywords:
Hematite (α-Fe_2O_3)
Hydrothermal synthesis
Nanostructures
Magnetic materials
Morin transition

ABSTRACT

We report on hydrothermal synthesis, plate-like morphology, microstructure and magnetic properties of hematite (α-Fe_2O_3) plate-like particles. The sample is obtained immediately after the hydrothermal process without using any template and without further heat treatment. The so-obtained sample is characterized by X-ray powder diffraction (XRPD), energy-dispersive X-ray spectroscopy (EDX), field-emission scanning electron microscope (FE-SEM), transmission electron microscopy (TEM), high-resolution TEM (HRTEM), and superconducting quantum interference device (SQUID) magnetometer. XRPD confirms the formation of a single-phase hematite sample whereas EDX reveals that iron and oxygen are the only components of the sample. SEM, FE-SEM, TEM and HRTEM show that the sample is composed of plate-like particles. The width of the particles is ~500 nm whereas thickness is ~100 nm (aspect ratio 5:1). The HRTEM images exhibit well defined lattice fringes of α-Fe_2O_3 particles that confirm their high crystallinity. Moreover, the HRTEM analysis indicates the plate-like particles preferring crystal growth along [0 1 2] direction. Magnetic measurements display significant hysteretic behavior at room temperature with coercivity H_C = 1140 Oe, remanent magnetization M_r = 0.125 emu/g and saturation magnetization M_S = 2.15 emu/g as well as the Morin transition at $T_M \sim 250$ K. The magnetic properties are discussed with respect to morphology and microstructure of the particles. The results and comparison with urchin-like, rods, spherical, hexagonal, star-like, dendrites, platelets, irregular, nanoplatelets, nanocolumns and nanospheres hematites reveal that the plate-like particles possess good magnetic properties. One may conjecture that the shape anisotropy plays an important role in the magnetic properties of the sample.

© 2011 Elsevier B.V. All rights reserved.

1. Introduction

During the last decade iron (III) oxides have been at the focus of a remarkable research interest due to a wide variety of properties, as well as possessing a huge potential for applications [1–20]. Among seven polymorphs of iron (III) oxide, α-Fe_2O_3 (hematite) in various forms (such as bare nanoparticles, nanowires, microcubes, rods, microspheres, nanorods, nanotubes, and nanoparticles embedded in an inert matrix) has been under extensive investigation in order to understand the influence of size, shape, anisotropy, microstructure, inter-particle interaction and surface effects on its physical properties.

Hematite (α-Fe_2O_3) is the most stable iron oxide with a high resistance to corrosion, low cost, environmentally friendliness and non-toxicity. It is used as a pigment, catalyst, sensor, electrode material, biomedical and magnetic material [1,2,21–23]. Hematite crystallizes in the rhombohedral system space group R-3c (corundum structure) with n-type semiconducting properties (2.1 eV band gap) [1,2]. Despite intensive research, some of its features are still not fully known. Some of these unknowns concern the magnetic properties [24–46]. Hematite's magnetic properties may display three critical temperatures: the Néel temperature, the Morin temperature, and the blocking temperature. In bulk hematite the Néel temperature is $T_N \approx 960$ K and the Morin transition takes place at the temperature $T_M \approx 263$ K [1]. Below T_M the spins are antiparallel and the material behaves as a uniaxial antiferromagnet (AF). Above T_M, the spins show slight canting and a small net magnetic moment appears (weak ferromagnetism, WF) [1]. As the particle size decreases the Morin temperature

* Corresponding author.
E-mail address: marint@vinca.rs (M. Tadić).

0925-8388/$ – see front matter © 2011 Elsevier B.V. All rights reserved.
doi:10.1016/j.jallcom.2011.04.117

is reduced, and tends to zero for particles smaller than about 8–20 nm [1,37,38,44–46]. If the particles become small enough, the direction of the magnetic moment in a single domain fluctuates due to thermal agitation, leading to superparamagnetic behavior above the blocking temperature T_B, and to spatial freezing of these moments below T_B [37]. It is well-known that the magnetic properties of α-Fe_2O_3 are also very sensitive to the morphology and microstructure of the samples [38–55]. Therefore, complex magnetic properties of hematite have been widely discussed and a wide range of magnetic properties has been obtained. Song et al. reported star-like like arrayed hematite particles and a weak ferromagnetic behavior with a remanent magnetization of 0.569 emu/g and coercivity of 156.08 Oe at room temperature [43]. Bharathi et al. reported three samples α-Fe_2O_3 with different morphologies and their magnetic properties at room temperature: dendrite (M_S = 2.534 emu/g, M_r = 0.202 emu/g and H_C = 157 Oe), single-layered snowflake (M_S = 1.379 emu/g, M_r = 0.119 emu/g and H_C = 239 Oe) and double-layered snowflake (M_S = 0.834 emu/g, M_r = 0.236 emu/g and H_C = 436 Oe) [47]. On the other hand, Liang and Wang synthesized micro-snowflake-like morphology with weak ferromagnetic property at room temperature (H_C = 134 Oe, M_r = 0.67 emu/g) [42]. A recent paper by Gupta et al. reported on hematite rods with nonzero coercivity H_C = 107 Oe and remanent magnetization M_r = 0.064 emu/g at room temperature, as well as dependence of the Morin transition on the applied magnetic field [48]. Darezereshki prepared hematite nano-particles by direct thermal-decomposition of maghemite with coercivity H_C = 101 Oe and remanent magnetization M_r = 0.00654 emu/g at room temperature [30], whereas Tsuzuki et al. prepared hematite nano-platelets by mechanochemical/thermal processing with H_C = 160 Oe and M_r = 0.2 emu/g at room temperature [27]. Moreover, the magnetic properties are strongly affected by the synthetic conditions and the search for methods capable of tailoring these parameters is a current research field. In this context, the development and improvement of the synthesis methods of materials is an effective strategy for modifying their properties. Various methods for the synthesis of hematite are reported, such as sol–gel, combustion, composite-hydroxide-mediated, template, aqueous solution-based, precipitation, oxalic acid etching process, high energy ball milling, alcohol-thermal reaction, solvothermal, thermal decomposition, catalytic and hydrothermal [1,2,14–21,37–63]. Among these techniques, hydrothermal is one of the most reliable and effective synthesis methods. The morphology and crystallinity in hydrothermal process can be controlled by varying parameters such as pressure, temperature, reaction time, solution pH value, reactant concentration, solvent, surfactant and precursor [1,10,16,19,21,26,28,31,39–42,61,62,64–68]. This technique provides relatively low process temperature and reduces processing time. Various morphologies of α-Fe_2O_3 such as stalactite-like, coral-like, cluster-like, cube, porous, snowflake-like, star-like, ring-like, urchin-like, hexagonal, nanotubes, nanoplatelets, nanorods, flower-like, nanospheres, nanoaggregates and nanorhombohedra with a wide range of the magnetic properties have been reported showing huge possibilities of the hydrothermal method [1,10,16,19,28,31,38,39,42,43,61–71]. However, only a few reports involve the formation of α-Fe_2O_3 plate-like structures [59,70–75].

In continuation of our research on α-Fe_2O_3 [35,37,38,46,76], in this paper we report on hydrothermal synthesis of α-Fe_2O_3 particles and their morphology, microstructure and magnetic properties. The investigation of the sample showed high phase purity of α-Fe_2O_3, well-crystallized sample, plate-like morphology with width ~ 500 nm and thickness ~ 100 nm, perfect lattice fringes of the particles, preferring crystal growth along [0 1 2] direction, the Morin transition at $T_M \approx 250$ K and hysteretic behavior at room temperature with coercivity H_C = 1140 Oe, remanent magnetization M_r = 0.125 emu/g and saturation magnetization

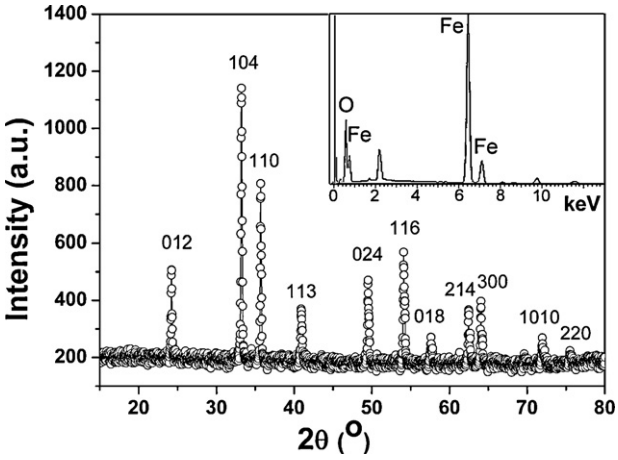

Fig. 1. X-ray diffraction pattern of the sample. The Miller indices (*h k l*) of the peaks are also shown. Inset: EDX spectrum of the α-Fe_2O_3 particles.

M_S = 2.15 emu/g. The motivation for this work was an investigation of hematite plate-like particles that have the potential importance in fundamental research as well as the technological applications. Moreover, plate-like particles have a large shape anisotropy and should therefore exhibit magnetic properties that have not been thoroughly examined. There are few reports about hematite with plate-like structures in the literature that investigate magnetic properties. The results of this work show that hematites with a plate-like morphology have better properties than some hematites with various shapes. Therefore, plate-like hematite particles should be subject of further investigations. Moreover, we have shown that the hydrothermal process provides an easy route to synthesis of hematite particles with a plate-like morphology.

2. Experimental

The α-Fe_2O_3 particles were prepared by the hydrothermal method: an appropriate preparation route was found for production of single-phase hematite plate-like structures. The starting point for the formation of the sample is a solution of deionised water and ethanol in ratio 1:1 (1 l). Next 0.2 mol of iron nitrate ($Fe(NO_3)_3 \cdot 9H_2O$, Aldrich 98%), 3 g of oleic acid and 0.5 mol of NaOH were added in the water/ethanol solution. The solution was mixed by stirring and then put in a 2 l Parr stainless steel hydrothermal reactor. The hydrothermal reactor was heated up to 200 °C and was held at that temperature for 1 h. Thereafter, it was quenched down to room temperature. Constant stirring of 800 rpm was applied during the hydrothermal process. Red powder was collected by centrifugation, washed four times in deionised water and ethanol, and dried at 80 °C for 4 h.

The X-ray powder diffractometer (Phillips PW-1710) employing CuKα (λ = 1.5406 Å, 2θ = 10–80°) radiation was used to characterize the crystal structure of the sample. The size and morphology of the iron oxide particles were observed with a FE-SEM (field-emission scanning electron microscope, Zeiss Supra 35VP). The size, morphology and microstructure were observed by TEM (transmission electron microscopy, JEOL 2010 F) operating at 200 kV. Elemental components were determined using energy-dispersive X-ray spectroscopy (EDX, Oxford Instruments, INCA PentaFETx3) provided in the SEM. Magnetic measurements were performed on a commercial Quantum Design MPMS-XL-5 SQUID-based magnetometer in a wide range of temperatures (5–300 K) and applied DC fields (up to 5 T).

3. Results and discussion

The structure and phase composition of the sample were determined by X-ray powder diffraction (XRPD) measurements (step 0.02°, exposition 15 s/step). The recorded and indexed diffraction pattern is depicted in Fig. 1 where sharp peaks can be observed, as expected for a highly crystalline sample. The positions of all the maxima coincide with the peaks characteristic of the hematite phase (JCPDS card 33-0664). No diffraction line corresponding to other phases has been observed, indicating a high purity of the sample. Inset of Fig. 1 shows the EDX spectrum of the sample where iron and oxygen are the main components. The atomic ratio of Fe

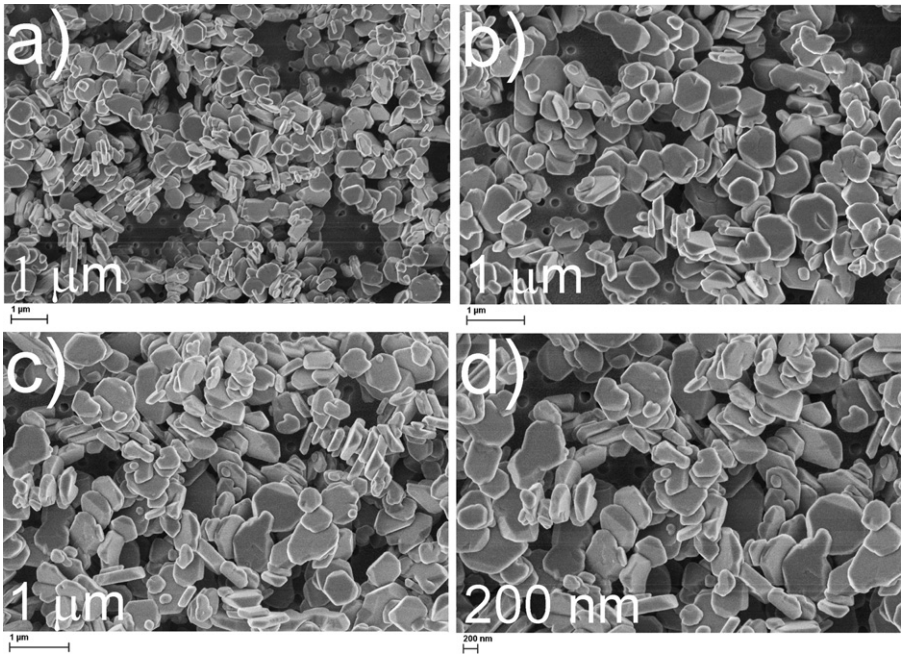

Fig. 2. FE-SEM images of the plate-like α-Fe_2O_3 particles.

and O is ~39:61 that is close to the stoichiometric composition of α-Fe_2O_3. The C, Au, Zn and Cu peaks in the EDX spectrum originate from the holder and paste which were used for the preparation of the sample for EDX observation. No other impurities have been identified.

The size, morphology and microstructure of the sample were characterized using FE-SEM, TEM and HRTEM techniques. The FE-SEM images of α-Fe_2O_3 particles are shown in Fig. 2(a)–(d). The figures clearly show that the sample is composed of plate-like particles. The width of the particles is ~500 nm whereas thickness is ~100 nm (Fig. 2). The aspect ratio is about 5:1. The corners of these hematite plate-like particles are rounded, with various curvatures. The surfaces of the particles are smooth. Moreover, TEM and HRTEM investigations give a deeper insight into the morphology and microstructure of the α-Fe_2O_3 particles. As shown in Fig. 3, a plate-like morphology of the individual α-Fe_2O_3 could be observed in TEM images. The TEM images clearly show particles in two perspectives: perpendicular and oblique perspective. The inset of Fig. 3(a) is selected area electron diffraction (SAED) pattern of the plate-like particles. The SAED of the particles shows a regular spot pattern, which confirms the single-crystalline nature of the plate-like particles. Fig. 4 shows HRTEM images of the plate-like particles. A HRTEM images (Fig. 4(a) and (b)) show perfect lattice fringes of selected regions of perpendicular perspective, that demonstrate good crystallization of particles. In addition, HRTEM images of oblique perspective are shown in Fig. 4(c) and (d) also showing good crystallinity. The observed lattice planes with a spacing of 0.37 (perpendicular perspective, shown in Fig. 4(b)) and

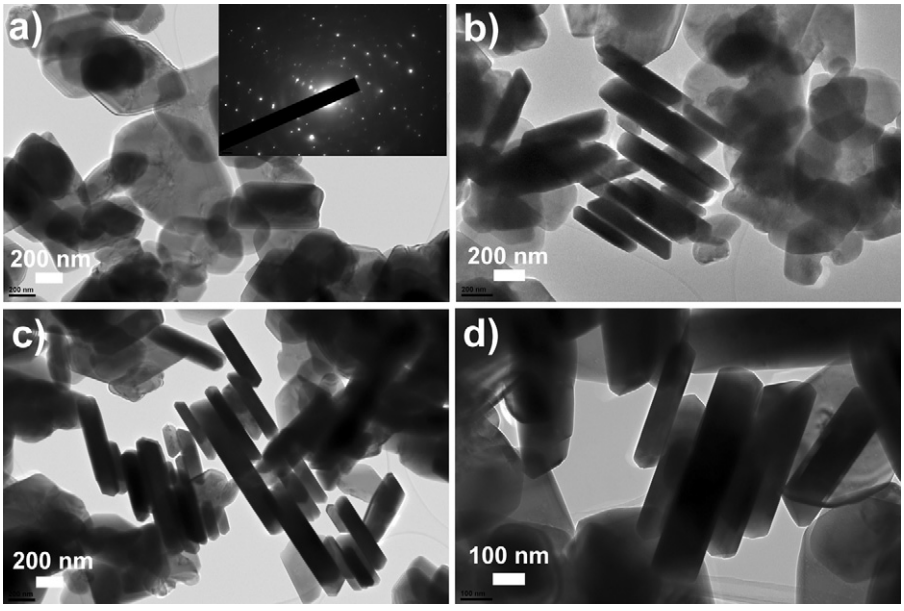

Fig. 3. (a)–(d) Transmission electron micrographs of the plate-like α-Fe_2O_3 particles: perpendicular and oblique perspectives. Inset shows selected electron diffraction pattern of the sample.

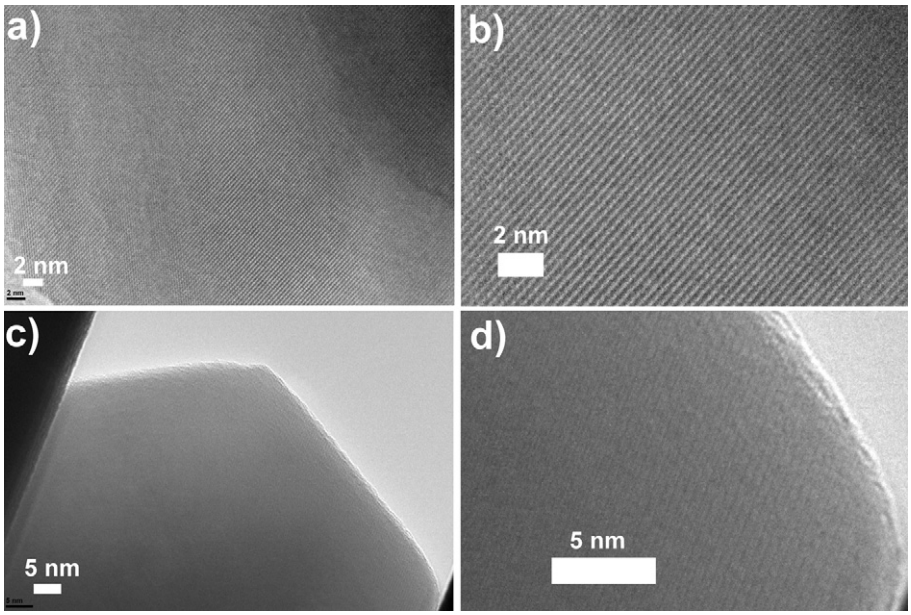

Fig. 4. (a)–(d) HRTEM images of the plate-like α-Fe_2O_3 particles. (a) and (b) are selected regions of the perpendicular perspective whereas (c) and (d) are selected regions of the oblique perspective.

0.22 nm (oblique perspective, shown in Fig. 4(d)) are consistent with the (0 1 2) and (1 1 3) planes of the hematite, respectively. The HRTEM analysis indicates the plate-like particles preferring crystal growth along [0 1 2] direction.

Magnetic properties of the sample were investigated by a SQUID magnetometer. The temperature dependence of the magnetization M(T) was measured in magnetic field $H = 1000$ Oe in zero-field-cooling (ZFC) and field-cooling (FC) modes as shown in Fig. 5. The M(T) (Fig. 5) of the α-Fe_2O_3 particles clearly shows their temperature dependence and a separation between the ZFC and FC curves. Such a divergence between the magnetization in a ZFC process and a FC process does not exist in bulk hematite and is characteristic of small particles [44,48,50]. A sharp increase of the magnetization at $T_M \approx 250$ K is clearly observed in both curves (ZFC and FC), which temperature may be assigned as the Morin temperature. The inset of Fig. 5 is the corresponding differential of the ZFC curve and the T_M is found to be 248.2 K. This, somewhat lower, value $T_M \approx 250$ K of the Morin transition temperature, obtained with the present sam-

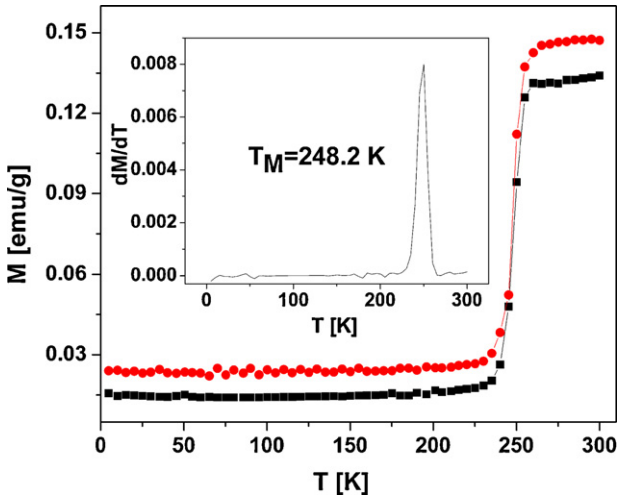

Fig. 5. Temperature dependence of the zero-field-cooled (ZFC, solid squares) and field-cooled (FC, solid circles) magnetization measured in a field of 1000 Oe. Inset is ZFC corresponding differential curve.

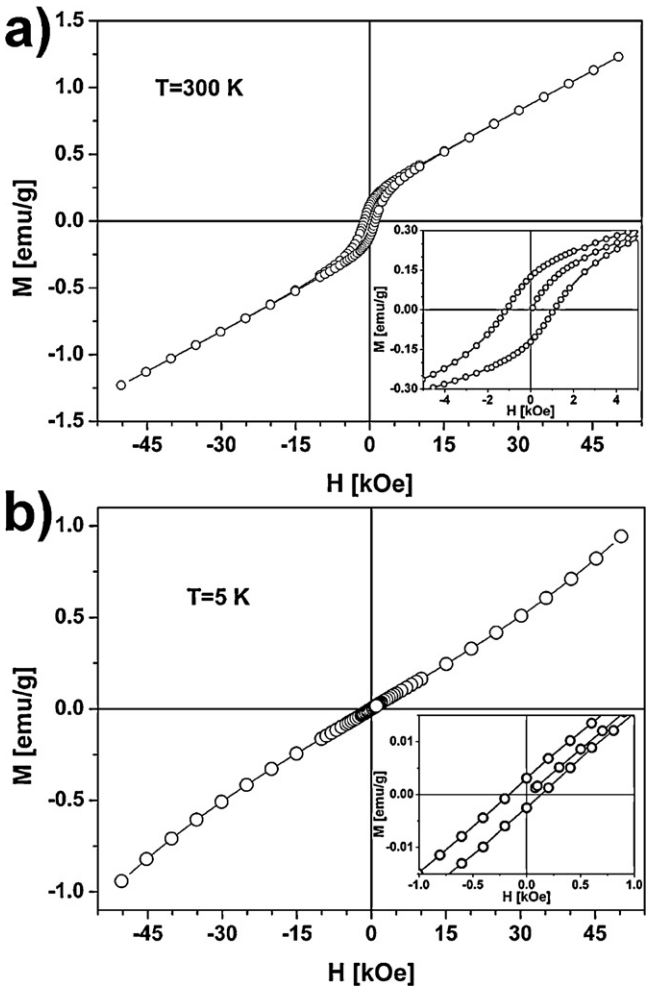

Fig. 6. The hysteresis loops of the α-Fe_2O_3 particles at room temperature (a) and 5 K (b). Insets show low field magnetization behavior.

Table 1
Comparative review of magnetic parameters at room temperature of several distinct hematite systems.

Morphology	Mean particle size	M_S (emu/g)	M_r (emu/g)	H_C (Oe)	Ref.
Urchin-like (nanorods)	$d \sim 80$ nm, $l \sim 800$ nm	~0.45 at 1 T	4.6783×10^{-3}	92.235	[65]
Rods	$l \sim 50$ μm	–	0.064	107	[48]
Spherical	$d \sim 100$ nm	11.05	1.798	155.76	[49]
Star-like	Length ~ 350 nm, width ~ 110 nm, thickness ~ 35 nm	–	0.569	156.08	[43]
Dendrites	Length ~ 5 μm	1.05 at 1.5 T	–	163	[83]
Hexagonal	$d \sim 100$ nm	0.494 at 1 T	0.077	185.28	[64]
Irregular	$d \sim 200$ nm	2 at 3 T	–	286	[82]
Hexagonal platelets	Edge length ~ 3 μm, thickness ~ 0.3 μm	–	0.11521	430.57	[81]
Nanoplatelets, Nanocolumns	$d \sim 120$ nm, heights ~ 50 nm$d \sim 80$ nm, heights ~ 130 nm	7.36 at 1 T, 10.32 at 1 T	1.72, 2.15	485, 550	[41]
Nanospheres	$d \sim 70$ nm	–	–	838.65	[80]
Plate-like	$d \sim 500$ nm, $t \sim 100$ nm	1.232 at 5 T, 2.15 at ∞ T	0.125	1140	This work

ple (Fig. 5) than the value obtained for bulk hematite $T_M \approx 263$ K can be explained as a consequence of its submicron form [44,48,50,79]. Below T_M the magnetizations (ZFC and FC) are almost constant down to 5 K. Fig. 6 shows the magnetic field dependence in the −5 T to 5 T range of the isothermal magnetization at room temperature (a) and 5 K (b). The existence of a hysteresis loop at room temperature, as well as the absence of magnetization saturation should be noticed (Fig. 6(a)). The M(H) curve at higher field shows almost linear dependence of magnetization on the applied magnetic field. The coercivity, remanent magnetization and saturation magnetization values are $H_C = 1140$ Oe, $M_r = 0.125$ emu/g and $M_S = 2.15$ emu/g, respectively. The value of M_S was determined by extrapolating $1/H$ to zero-field in the M vs. $1/H$ plot based on the high field data. Hysteretic behavior shows a weak ferromagnetic state (WF region) of the sample at room temperature (Fig. 6(a)). In Fig. 6(b), the M(H) data of the sample at 5 K are shown, exhibiting behavior of a antiferromagnetic material. However, a small hysteresis loop (inset of Fig. 6(b)) with the remanent magnetization $M_r = 0.0027$ emu/g and coercivity $H_C = 150$ Oe is observed in the sample at 5 K. These values are much smaller than the corresponding values at room temperature. The existence of the hysteresis loop below T_M (AF region) shows that uncompensated spins exist at the surface of particles.

The influence of the shape and microstructure of the particles on the coercivity is well known and an increase of the coercivity with increasing aspect ratio has been reported [26–34,39–43,47,55,78]. For example, in nanosized Fe, increases of aspect ratio by a factor 5 (from one to five) increases coercivity ten times [78]. Moreover, Mitra et al. reported the coercivity dependence on the shape of the hematite nanocrystals, $H_C \sim 330$ Oe (nanocube) < $H_C \sim 390$ Oe (nanospindle) < $H_C \sim 1250$ Oe (nanorhombohedra) [53]. In general, the coercivity increases with the increase of aspect ratio, i.e. with an increase of shape anisotropy. Spherically shaped crystals do not have any net shape anisotropy (aspect ratio ~ 1). In addition, Table 1 provides a comparative review of values of H_C, M_r and M_S for different α-Fe_2O_3 forms. The dependence of the magnetic properties on the morphology is noticeable and the shape anisotropy may play important role in the magnetic properties of samples in Table 1. It is interesting that the α-Fe_2O_3 plate-like particles reveal higher coercivity in comparison with the hematite urchin-like, rods, spherical, hexagonal, star-like, dendrites, platelets, irregular, nanoplatelets, nanocolumns and nanospheres (Table 1), i.e. an improvement in coercivity can be seen in the plate-like particles. On the basis of the above comparisons, it can be concluded that the plate-like particles possess good magnetic properties. Moreover, on the basis of the above listed results and the discussion it also can be concluded that the system under consideration (aspect ratio 5:1) shows the effects of the shape anisotropy on the magnetic properties which can increase the coercivity. Good magnetic properties and high coercivity at room temperature are also obtained in maghemite plate-like particles [77]. It is well known that, in particles with aspect ratio higher than one, the magnetic spins are preferentially aligned along the long axes and their reversal to the opposite direction requires higher energies in comparison with spherical particles [44]. The plate-like morphology may improve the magnetic property of hematite.

4. Conclusions

In summary, plate-like hematite particles were prepared by one-step template-free hydrothermal route using iron nitrate, oleic acid, ethanol and deionised water as starting materials. This method has the advantage of being simple, and allowing an easy production of highly crystalline hematite particles. The XRPD, EDX, FE-SEM, TEM and HRTEM measurements reveal pure phase of the α-Fe_2O_3 and the submicron plate-like morphology of the sample. The micrographs show a width of ~500 nm and a thickness of ~100 nm (aspect ratio 5:1) of the plate-like particles. The HRTEM shows perfect lattice fringes and preferential crystal growth along the [0 1 2] direction. The values of the coercivity, remanent magnetization and saturation magnetization at room temperature are $H_C = 1140$ Oe, $M_r = 0.125$ emu/g and $M_S = 2.15$ emu/g, respectively. Moreover, the Morin temperature is observed at $T_M \approx 250$ K that is lower than in bulk hematite showing sized effect. The obtained coercivity in the sample is higher than that of the hematite urchin-like, rods, spherical, hexagonal, star-like, dendrites platelets, irregular, nanoplatelets, nanocolumns and nanospheres (Table 1). We conjecture that the higher coercivity in the sample may be associated with the unique morphology of α-Fe_2O_3 particles because shape anisotropy can exert a high influence on their magnetic properties. Experimental investigation of the sample and comparison with various α-Fe_2O_3 forms indicate that the plate-like particles may improve magnetic properties of materials. In addition, it is still unclear how the microstructure, morphology, and magnetic properties are correlated in this material and demands further investigations.

Acknowledgements

M.T. acknowledges Professor Veljko Dmitrasinović (Institute for Physics, Belgrade) for his comments. The Serbian Ministry of Science has supported this work financially under grant no. III 45015.

References

[1] A.S. Teja, P.Y. Koh, Prog. Cryst. Growth Charact. Mater. 55 (2009) 22.
[2] M. Mahmoudi, A. Simchi, M. Imani, J. Iran. Chem. Soc. 7 (2010) S1.
[3] S.S. Shinde, C.H. Bhosale, K.Y. Rajpure, J. Alloys Compd. 509 (2011) 3943.
[4] M.A. Garcia-Lobato, A.I. Martinez, M. Castro-Roman, C. Falcony, L. Escobar-Alarcon, Physica E 406 (2011) 1496.
[5] G. Tong, W. Wu, J. Guan, H. Qian, J. Yuan, W. Li, J. Alloys Compd. 509 (2011) 4320.
[6] S.K. Sharma, J.M. Vargas, K.R. Pirota, S. Kumar, C.G. Lee, M. Knobel, J. Alloys Compd. 509 (2011) 6414.

[7] V.R Elias, M.I. Oliva, E.G. Vaschetto, S.E. Urreta, G.A. Eimer, S.P. Silvetti, J. Magn. Magn. Mater. 322 (2010) 3438.
[8] L.H. Han, H. Liu, Y. Wei, Powder Technol. 207 (2011) 42.
[9] P.M. Kulal, D.P. Dubal, C.D. Lokhande, V.J. Fulari, J. Alloys Compd. 509 (2011) 2567.
[10] Z. Liu, Y. Zheng, Powder Technol. 209 (2011) 119.
[11] A. Hassanjani-Roshan, M.R. Vaezi, A. Shokuhfan, Z. Rajabali, Particuology 9 (2011) 95.
[12] T. Tsuzuki, F. Schaffel, M. Muroi, P.G. McCormick, J. Alloys Compd. 509 (2011) 5420.
[13] O. Crisan, A.D. Crisan, J. Alloys Compd. 509 (2011) 6522.
[14] Y. Sun, G. Guo, B. Yang, W. Cai, Y. Tian, M. He, Y. Liu, Physica B 406 (2011) 1013.
[15] D. Wang, Q. Wang, T. Wang, Nanotechnology 22 (2011) 135604.
[16] L. Wang, L. Gao, Cryst. Eng. Commun. 13 (2011) 1998.
[17] Z. Cheng, J. Xu, H. Zhong, Y. Yang, W. Chen, Superlattice Microstruct. 47 (2010) 253.
[18] L.P. Zhu, G.H. Liao, N.C. Bing, X. Zhao, Y.Y. Gu, Mater. Lett. 65 (2011) 1287.
[19] C. Su, H. Wang, X. Liu, Cryst. Res. Technol. 46 (2011) 209.
[20] X. Huang, J. Guan, Z. Xiao, G. Tong, F. Mou, X. Fan, J. Colloid Interface Sci. 357 (2011) 36.
[21] G. Wang, T. Liu, Y. Luo, Y. Zhao, Z. Ren, J. Bai, H. Wang, J. Alloys Compd. (2011), doi:10.1016/j.jallcom.2011.03.151.
[22] J Singh, M. Srivastava, J. Dutta, P.K. Dutta, Int. J. Biol. Macromol. 48 (2011) 170.
[23] M.F. Hassan, Z. Guo, Z. Chen, H. Liu, Mater. Res. Bull. 46 (2011) 858.
[24] K Bachari, A. Touileb, A. Saadi, D. Halliche, O. Cherifi, J. Porous Mater. 17 (2010) 573.
[25] F.Y. Jiang, C.M. Wang, Y. Fu, R.C. Liu, J. Alloys Compd. 503 (2010) L31.
[26] X. Guo, S. Zhong, J. Zhang, W. Wang, J.J. Mao, G. Xie, J. Mater. Sci. 45 (2010) 6467.
[27] T. Tsuzuki, F. Schaffel, M. Muroi, P.G. McCormick, Powder Technol. (2011), doi:10.1016/j.powtec.2011.03.012.
[28] H. Wang, W. Geng, Y. Wang, Res. Chem. Intermed. 37 (2011) 389.
[29] M. Reufer, H. Dietsch, U. Gasser, B. Grobety, A.M. Hirt, V.K. Malik, P. Schurtenberger, J. Phys.: Condens. Matter 23 (2011) 065102.
[30] E. Darezereshki, Mater. Lett. 65 (2011) 642.
[31] W. Wu, X. Xiao, S. Zhang, J. Zhou, L. Fan, F. Ren, C. Jiang, J. Phys. Chem. C 114 (2010) 16092.
[32] R.K. Gupta, K. Ghosh, L. Dong, P.K. Kahol, Physica E 43 (2011) 1095.
[33] S. Bharathi, D. Nataraj, D. Mangalaraj, Y. Masuda, K. Senthil, K. Yong, J. Phys. D: Appl. Phys. 43 (2010) 015501.
[34] P. Guo, Z. Wei, B. Wang, Y. Ding, H. Li, G. Zhang, X.S. Zhao, Colloids Surf. A: Physicochem. Eng. Aspects 380 (2011) 234.
[35] M Tadic, V. Kusigerski, D. Markovic, I. Milosevic, V. Spasojevic, Mater. Lett. 63 (2009) 1054.
[36] V. Zelenak, A. Zelenakova, J. Kovac, U. Vainio, N. Murafa, J. Phys. Chem. C 113 (2009) 13045.
[37] M. Tadić, D. Marković, V. Spasojević, V. Kusigerski, M. Remškar, J. Pirnat, Z. Jagličić, J. Alloys Compd. 441 (2007) 291.
[38] M. Tadić, V. Kusigerski, D. Marković, N. Čitaković, M. Remškar, V. Spasojević, J. Alloys Compd. 486 (2009) 839.
[39] S. Mandal, A.H.E. Muller, Mater. Chem. Phys. 111 (2008) 438.
[40] X. Xie, H. Yang, F. Zhang, L. Li, J. Ma, H. Jiao, J. Zhang, J. Alloys Compd. 477 (2009) 90.
[41] Q.-j. Sun, X.-g. Lu, G.-y. Liang, Mater. Lett. 64 (2010) 2006.
[42] H.F. Liang, Z.C. Wang, Mater. Lett. 64 (2010) 2410.
[43] F. Song, J. Guan, X. Fan, G. Yan, J. Alloys Compd. 485 (2009) 753.
[44] Z. Li, X. Lai, H. Wang, D. Mao, C. Xing, D. Wang, Nanotechnology 20 (2009) 245603.
[45] A. Zelenakova, J. Kovac, V. Zelenak, J. Appl. Phys. 108 (2010) 034323.
[46] M. Tadic, V. Kusigerski, D. Markovic, I. Milosevic, V. Spasojevic, J. Magn. Magn. Mater. 321 (2009) 12.
[47] S. Bharathi, D. Nataraj, M. Seetha, D. Mangalaraj, N. Ponpandian, Y. Masuda, K. Senthil, K. Yong, Cryst. Eng. Commun. 12 (2010) 373.
[48] R.K. Gupta, K. Ghosh, L. Dong, P.K. Kahol, Mater. Lett. 65 (2011) 225.
[49] X. Wang, L. Zhang, N. Yonghong, J. Hong, X. Cao, J. Phys. Chem. C 113 (2009) 7003.
[50] C. Xia, C. Hu, Y. Xiong, N. Wang, J. Alloys Compd. 480 (2009) 970.
[51] P.P. Sarangi, S.R. Vadera, M.K. Patra, C. Prakash, N.N. Ghosh, J. Am. Ceram. Soc. 92 (2009) 2425.
[52] J. Jacob, M.A. Khadar, J. Magn. Magn. Mater. 322 (2010) 614.
[53] S. Mitra, S. Das, K. Mandal, S. Chaudhuri, Nanotechnology 18 (2007) 275608.
[54] H. Liu, Y. Wei, P. Li, Y. Zhang, Y. Sun, Mater. Chem. Phys. 102 (2007) 1.
[55] M. Cao, T. Liu, S. Gao, G. Sun, X. Wu, C. Hu, Z.L. Wang, Angew. Chem. Int. Ed. 44 (2005) 4197.
[56] G. Wu, X. Tan, G. Li, C. Hu, J. Alloys Compd. 504 (2010) 371.
[57] O.M. Lemine, M. Sajieddine, M. Bououdina, R. Msalam, S. Mufti, A. Alyamani, J. Alloys Compd. 502 (2010) 279.
[58] S.W. Cao, Y.J. Zhu, G.F. Cheng, Y.H. Huang, J. Phys. Chem. Solids 71 (2010) 1680.
[59] L. Chen, X. Yang, J. Chen, J. Liu, H. Wu, H. Zhang, C. Liang, M. Wu, Inorg. Chem. 49 (2010) 8411.
[60] J.S. Chen, T. Zhy, X.H. Yang, H.G. Yang, X.W. Lou, J. Am. Chem. Soc. 132 (2010) 13162.
[61] X. Zhang, Q. Li, Mater. Lett. 62 (2008) 988.
[62] D. Wang, C. Song, Y. Zhao, M. Yang, J. Phys. Chem. C 112 (2008) 12710.
[63] L. Li, Y. Chu, Y. Liu, Nanotechnology 18 (2007) 105603.
[64] J. Hua, J. Gengsheng, Mater. Lett. 63 (2009) 2725.
[65] L.P. Zhu, H.M. Xiao, X.M. Liu, S.Y. Fu, J. Mater. Chem. 16 (2006) 1794.
[66] Y.C. Zhang, J.Y. Tang, X.Y. Hu, J. Alloys Compd. 462 (2008) 24.
[67] C.J. Jia, L.D. Sun, Z.G. Yan, L.P. You, F. Luo, X.D. Han, Y.C. Pang, Z. Zhang, C. Yan, Angew. Chem. Int. Ed. 44 (2005) 4328.
[68] J. Zhang, Y. Cheng, Q. Yang, Mater. Lett. 63 (2009) 2075.
[69] L.S. Zhong, J.S. Hu, H.P. Liang, A.M. Cao, W.G. Song, L.J. Wan, Adv. Mater. 18 (2006) 2426.
[70] M. Srivastava, A.K. Ojha, S. Chaubey, J. Singh, P.K. Sharma, A.C. Pandey, J. Alloys Compd. 500 (2010) 206.
[71] W. Yin, X. Chen, M. Cao, C. Hu, B. Wei, J. Phys. Chem. C 113 (2009) 15897.
[72] J. Wu, H. Zhang, N. Du, X. Ma, D. Yang, J. Phys. Chem. B 110 (2006) 11196.
[73] S.L. Zhong, J.M. Song, S. Zhang, H. Yao, A.W. Xu, W.T. Yao, S.H. Yu, J. Phys. Chem. C 112 (2008) 19916.
[74] G.Y. Zhang, Y.Y. Xu, D.Z. Gao, Y.Q. Sun, J. Alloys Compd. 509 (2011) 885.
[75] S. Liu, J. Zhou, L. Zhang, J. Phys. Chem. C 115 (2011) 3602.
[76] M. Tadic, V. Spasojevic, V. Kusigerski, D. Markovic, M. Remskar, Scripta Mater. 58 (2008) 703.
[77] W.D. Zhang, H.M. Xiao, L.P. Zhu, S.Y. Fu, J. Alloys Compd. 477 (2009) 736.
[78] A.H. Lu, E.L. Salabas, F. Schuth, Angew. Chem. Int. Ed. 46 (2007) 1222.
[79] H.M. Lu, X.K. Meng, J. Phys. Chem. C 114 (2010) 21291.
[80] L. Sun, M. Cao, C. Hu, Solid State Sci. 12 (2010) 2020.
[81] D. Peng, S. Beysen, Q. Li, Y. Sun, L. Yang, Particuology 8 (2010) 386.
[82] M.M. Can, T. Firat, S. Ozcan, Physica B (2011), doi:10.1016/j.physb.2011.01.002.
[83] J. Liang, L. Li, W. Song, J. Fang, M. Luo, Y. Li, Cryst. Res. Technol. 45 (2010) 405.